Correlations in two-dimensional vortex liquids

Jun Hu and A. H. MacDonald
Department of Physics, Indiana University, Bloomington, Indiana 47405

B. D. McKay
Computer Science Department, Australian National University, Canberra, Australian Capital Territory 0200, Australia
(Received 16 February 1994)

We report on a high-temperature perturbation expansion study of the superfluid-density spatial correlation function of a Ginzburg-Landau-model superconducting film in a magnetic field. We have derived a closed form which expresses the contribution to the correlation function from each graph of the perturbation theory in terms of the number of Euler paths around appropriate subgraphs. We have enumerated all graphs appearing out to 12th order in the expansion and have evaluated their contributions to the correlation function. Low-temperature correlation functions, obtained using Padé approximants, are in good agreement with Monte Carlo simulation results and show that the vortex liquid becomes strongly correlated at temperatures well above the vortex solidification temperature. We have also evaluated the high-temperature expansion for the free energy of the Ginzburg-Landau model to 13th order, two orders further than in previous work.

I. INTRODUCTION

Because of the combination of high transition temperatures, strong anisotropy, and short coherence lengths which occurs in high-temperature superconductors, strong thermal fluctuations are present over a wide temperature interval in these materials. Thermal fluctuations are especially important in a magnetic field where they are responsible for the melting of the Abrikosov[1] vortex lattice at temperatures below the mean-field critical temperature giving rise to a vortex liquid state.[2] In this paper we report on a study of correlations in the vortex liquid in the extreme anisotropy limit of decoupled layers. We have evaluated the leading terms in the high-temperature perturbation expansion of the superfluid-density spatial correlation function for the Ginzburg-Landau model of a superconductor film.

The thermodynamics of this system is unusual because of Landau quantization of the order parameter fluctuations;[3] our calculations are carried out within the lowest Landau level approximation in which only the lowest gradient energy fluctuations are retained. This approximation is valid near the mean-field transition temperature and is ordinarily valid throughout the vortex liquid state, although fluctuation effects may be strong enough in some high-temperature superconductors to drive the solidification transition outside of its range of validity. High-temperature perturbation expansions for the free energy of this model, even when evaluated to high order,[4,5] exhibit little evidence of the Abrikosov vortex lattice state which is expected to occur at low temperatures. Recent Monte Carlo simulations,[6–9] on the other hand, generally obtain results indicative of a weak first-order phase transition between the two states. (See, however, Ref. 9 where a different conclusion is reached.) We find that the perturbation expansion for the superfluid-density correlation function, unlike that for the average superfluid density studied by previous workers,[4,5] provides clear evidence of strong correlations in the vortex liquid which presage the appearance of an ordered state at low temperatures.

The paper is organized as following. In Sec. II we introduce the quantity we study, $\langle|\Delta(\vec{q})|^2\rangle$ which is proportional to the Fourier transform of the superfluid-density spatial correlation function. In Sec. III we outline the high-temperature perturbation expansion for this quantity and present our closed form result for the contribution to it from individual diagrams which appear in the expansion. In Sec. IV we discuss our evaluation of all terms out to twelfth order in this expansion and discuss some comparisons with expansions for the free energy performed by earlier workers which allow us to check our results. Extrapolations of our finite-order results to low temperatures using Padé approximants are presented and compared with Monte Carlo simulations. In Sec. V we discuss our results on the high-temperature expansion for the free energy. We have evaluated the coefficients of this expansion exactly out to 13th order, two orders further than in the most recent prior work.[4,5] Previous workers speculated on the basis of existing results that the zero-temperature limits of Padé approximants to the free energy series extrapolated to the exact zero-temperature free energy in the limit of infinite-order approximants. Our results allow us to determine an approximant of one higher order than was previously possible and do not support this speculation. Section VI contains a brief summary.

II. SUPERFLUID-DENSITY CORRELATION FUNCTION

The free energy per unit area of the Ginzburg-Landau-model superconducting film in a perpendicular magnetic

field is given by

$$f[\Psi] = \alpha(T)|\Psi|^2 + \frac{\beta}{2}|\Psi|^4 + \frac{1}{2m}|(-i\hbar\nabla - 2e\vec{A})\Psi|^2, \quad (1)$$

where $\Psi(\vec{r})$ is the order parameter. $\Psi(\vec{r})$ is proportional to the wave function for the center of mass of the Cooper pairs[10] and $\vec{B} = \nabla \times \vec{A}$. [We employ the Landau gauge so that $\vec{A} = (0, Bx, 0)$.] The quadratic terms in Eq. (1) are minimized by order parameters which correspond to a lowest Landau level (LLL) wave function for the Cooper pairs. In using Eq. (1) we are neglecting screening so that $\vec{B}$ is the external magnetic field. This approximation is valid for type-II superconductors near the upper critical field, the regime of interest in this article. The mean-field-theory superconducting instability occurs when the quadratic terms in Eq. (1) become negative for the LLL, i.e., at $T_c^{\rm MF}$ where $\alpha_H(T_c^{\rm MF}) = 0$ ($\alpha_H \equiv \alpha + \hbar eB/m^*$). In the LLL approximation we assume that fluctuations in higher Landau level channels can be neglected or at least absorbed in a renormalization of $\alpha(T)$.[4,6,11,12] Then the order parameter $\Psi(\vec{r})$ can be expanded as

$$\Psi(\vec{r}) = \sum_p C_p (L_y)^{-1/2} \left(\frac{2eB}{\pi\hbar}\right)^{1/4} e^{ipy} e^{-\frac{eB}{\hbar}(x - \frac{\hbar p}{2eB})^2}, \quad (2)$$

where the number of terms in the sum over p is $N_\phi = L_x L_y/2\pi\ell^2 = L_x L_y(eB/\pi\hbar)$. This expansion leads to the following expression for the Ginzburg-Landau model free energy:

$$\int f[\Psi]d\vec{r} = \left(\alpha_H \sum_p |C_p|^2 + \frac{\beta}{2} \sum_{p_1 p_2 p_3 p_4} (L_y)^{-1}(2\pi\ell^2)^{-1/2} \times \exp\left\{-\frac{\ell^2}{2}\left[\sum_{i=1}^4 p_i^2 - \frac{1}{4}\left(\sum_{i=1}^4 p_i\right)^2\right]\right\} \times \bar{C}_{p_1}\bar{C}_{p_2}C_{p_3}C_{p_4}\delta_{p_1+p_2,p_3+p_4}\right), \quad (3)$$

where $\alpha_H = \alpha(T)[1 - H/H_{c2}(T)]$. Fluctuation effects in the model are regulated by the dimensionless parameter $g \equiv \alpha_H(\pi\ell^2/\beta k_B T)^{1/2}$.

The central quantity in our work is the superfluid-density spatial correlation function which we define by

$$\chi_{\rm SFD}(\vec{R}) \equiv \langle|\Psi(\vec{r})|^2|\Psi(\vec{r}+\vec{R})|^2\rangle - \langle|\Psi(\vec{r})|^2\rangle\langle|\Psi(\vec{r}+\vec{R})|^2\rangle. \quad (4)$$

Translational invariance of the system guarantees that the right hand side of Eq. (4) is independent of $\vec{r}$. The modulation of the average superfluid density when the homogeneous system is disturbed by weak pinning can be expressed in terms of $\chi_{\rm SFD}(\vec{R})$:

$$\delta\langle|\Psi(\vec{r})|^2\rangle = \frac{-1}{k_B T}\int d\vec{r}\,'\chi_{\rm SFD}(\vec{r}\,' - \vec{r})\delta\alpha(\vec{r}\,'), \quad (5)$$

where $\delta\alpha(\vec{r}\,')$ reflects the modulation of the mean-field transition temperature by pinning. The Fourier transform of $\chi_{\rm SFD}(\vec{r})$ is

$$\chi_{\rm SFD}(\vec{q}) \equiv \frac{1}{L_x L_y}\int d^2\vec{r}\int d^2\vec{r}\,'[\langle|\Psi(\vec{r})|^2|\Psi(\vec{r}\,')|^2\rangle - \langle|\Psi(\vec{r})|^2\rangle\langle|\Psi(\vec{r}\,')|^2\rangle]\exp[i\vec{q}\cdot(\vec{r}-\vec{r}\,')]. \quad (6)$$

We evaluate $\chi_{\rm SFD}(\vec{q})$ by expressing it in terms of

$$\Delta(\vec{q}) \equiv \frac{1}{N_\phi}\sum_{p_1 p_2}\bar{C}_{p_1}C_{p_2}\delta_{p_2,p_1+q_y} \times \exp[-i\ell^2 q_x(p_1+p_2)/2], \quad (7)$$

so that

$$\chi_{\rm SFD}(\vec{q}) = \frac{N_\phi^2}{L_x L_y}[\exp(-q^2\ell^2/2)\langle|\Delta(\vec{q})|^2\rangle - \langle\Delta(\vec{q}=0)\rangle^2]. \quad (8)$$

$\Delta(\vec{q})$ satisfies the following informative sum rule[8] for each configuration of the Ginzburg-Landau system,

$$\frac{1}{N_\phi}\sum_{\vec{q}}[|\tilde{\Delta}(\vec{q})|^2 - 1/N_\phi] = 0, \quad (9)$$

where $\tilde{\Delta}(\vec{q}) \equiv \Delta(\vec{q})/\Delta_0$ and $\Delta_0 \equiv \Delta(\vec{q}=0)$ is proportional to the integrated superfluid density.[13] [Note that $\tilde{\Delta}(\vec{q})$ is invariant when the order parameter is multiplied by an overall constant.] $\langle|\tilde{\Delta}(\vec{q})|^2\rangle$ is a particularly revealing quantity to examine in studying correlations in the vortex liquid. Equation (9) guarantees that (for large N_ϕ) $\lim_{q\to\infty} N_\phi|\tilde{\Delta}(\vec{q})|^2 = 1$ for any vortex liquid configuration. For example, in the high-temperature (vortex gas) limit $\langle|\tilde{\Delta}(\vec{q})|^2\rangle = 1/N_\phi$ for all $\vec{q} \neq \vec{0}$. On the other hand it is easy to show that in the low temperature limit the mean-field Abrikosov lattice configuration of the order parameter gives

$$|\tilde{\Delta}(\vec{q})|^2 = \begin{cases} 1 & \text{at } \vec{q} = \vec{G}, \\ 0 & \text{otherwise}, \end{cases} \quad (10)$$

where G is any reciprocal lattice vector. Thus $N_\phi\langle|\tilde{\Delta}(\vec{q})|^2\rangle \equiv s_V(q)$ shows exactly the behavior which would be expected for the static structure function of a classical fluid with N_ϕ particles in both low-temperature (solid) and high-temperature (gas) limits. It seems clear that $s_V(q)$ must be closely related to the static structure factor of the zeros of the order parameter, the vortices, although we do not believe that they are identical at all temperatures. For the purposes of the present study it is sufficient to observe that $h_V(q) \equiv s_V(q) - 1$, which we call the vortex correlation function, is a convenient measure of the degree of correlation in this system.

III. HIGH-TEMPERATURE PERTURBATION EXPANSION

$|\Delta(\vec{q})|^2$ can be expressed in the form

$$|\Delta(\vec{q})|^2 = N_\phi^{-2} \sum_{p_1 p_2 p_3 p_4} \bar{C}_{p_1}\bar{C}_{p_2}C_{p_3}C_{p_4}\delta_{p_1+p_2,p_3+p_4} \times(\delta_{p_1,p_4+q_y} e^{i\ell^2 q_x(p_4-p_2)}). \quad (11)$$

At high temperatures we can evaluate its thermal average

$$\langle|\Delta(\vec{q})|^2\rangle \equiv \frac{1}{Z}\int\prod_p d\bar{C}_p dC_p |\Delta(\vec{q})|^2 e^{-\frac{\alpha_H}{k_B T}\int d\vec{r}|\Psi|^2} \times e^{-\frac{\beta}{2k_B T}\int d\vec{r}|\Psi|^4}, \quad (12)$$

where Z is the partition function

$$Z = \int\prod_p d\bar{C}_p dC_p e^{-\frac{\alpha_H}{k_B T}\int d\vec{r}|\Psi|^2} \times e^{-\frac{\beta}{2k_B T}\int d\vec{r}|\Psi|^4}, \quad (13)$$

by expanding the contribution to thermal weighting factors from the quartic contribution to the Landau-Ginzburg free energy. The perturbation series can most easily be handled in terms of Feynman diagrams.[4,14] At nth order, there are contributions from diagrams with $(n+1)$ vertices and $2(n+1)$ edges in which the edges represent the Gaussian approximation correlation functions, n vertices represent $|\Psi|^4$ terms proportional to β, and the additional "external" vertex corresponds to $|\Delta(\vec{q})|^2$. An important consequence of the Landau quantization of order parameter fluctuations is the fact that the Gaussian approximation correlation functions,

$$\langle\bar{C}_{p'}C_p\rangle = \delta_{p',p}k_B T/\alpha_H, \quad (14)$$

are independent of the momentum p. Each vertex has two directed outgoing lines to represent the factors of C_p associated with it and two incoming lines to represent the factors of $\bar{C}_p$. All diagrams containing single-loop dressings of edges or vertices (except the external vertex) can be eliminated by following Ruggeri and Thouless[4] and expanding in terms of "Hartree-Fock" approximation correlation functions. This renormalization replaces[4] α_H in Eq. (14) by $\tilde{\alpha} \equiv -2\alpha_H/(g^2 \pm [g^4+4g^2]^{1/2})$. [The $+$ $(-)$ sign applies for $g<0$ $(g>0)$.] $\tilde{\alpha}$ remains positive for all temperatures so that the renormalized expansion parameter of the high-temperature perturbation expansion, $x \equiv (\beta k_B T)/(4\pi\ell^2\tilde{\alpha}^2)$, remains finite at all temperatures. [$\tilde{\alpha} \approx \alpha_H$ for $g \gg 0$, $\tilde{\alpha} \approx |\alpha_H|/g^2$ for $g \ll 0$; $\tilde{\alpha} = \alpha_H(1-4x)^{-1}$, $g^2 = (4x-1)^2/4x$ and $x = 1/4$ at $T_c^{\rm MF}$.] When the expansion is performed in terms of the Hartree-Fock correlation functions, $\langle|\Delta(\vec{q})|^2\rangle$ is the sum of all the connected diagrams without single-loop dressings except at the external vertex.

It is convenient to label the external vertex as vertex 1 and to label the incoming momenta at vertex i as p_{2i} and p_{2i-1}. Then the contribution to $\langle|\Delta(\vec{q})|^2\rangle$ from an nth-order diagram is given by $(k_B T/\tilde{\alpha})^2(-x)^n N_\phi^{-1} I(\vec{q})/n!$ where

$$I(\vec{q}) \equiv e^{-i\ell^2 q_y(q_x+iq_y)}\left(\frac{2\pi}{\ell^2}\right)^{-n/2}\sum_{p_2}\int dp_3\cdots\int dp_{2n+2}\prod_{\mu=2}^{n+1}\delta\left(\sum_i (M_{\mu i}-N_{\mu i})p_i\right) \times(\delta_{p_1'+q_y}+\delta_{p_2'+q_y})e^{-i\ell^2(q_x+iq_y)p_2}\exp\left\{-\frac{\ell^2}{2}\sum_{\mu=2}^{n+1}(p_{2\mu}-p_{2\mu-1})^2\right\}, \quad (15)$$

p_1' and p_2' are the two outgoing momentum labels at vertex 1, μ labels the vertices, and $M_{\mu i}$ is unity if i goes into the vertex μ and is zero otherwise, while $N_{\mu i}$ is unity if i comes out of μ and is zero otherwise.[4] To obtain this result we have noted that the integral is invariant under a shift of all momenta, set $p_1 = 0$, and multiplied by N_ϕ. It turns out that the integral $I(\vec{q})$ can be evaluated exactly and expressed in terms of the number of Euler paths in the two subgraphs obtained by deleting the external vertex and making the possible contractions. The two contractions correspond to the two δ functions which fix either p_1' or p_2' in Eq. (15). We denote the Euler path numbers for the two subgraphs by T^A and T^B. The following result is derived in the Appendix A:

$$I(\vec{q}) = \left\{\frac{1}{T^A}\exp\left(-\frac{T^B}{2T^A}q^2\ell^2\right) + \frac{1}{T^B}\exp\left(-\frac{T^A}{2T^B}q^2\ell^2\right)\right\} \quad (16)$$

if $T^A \times T^B \neq 0$, and

$$I(\vec{q}) = (N_\phi\delta_{\vec{q},0}+1)/(T^A+T^B) \quad (17)$$

if $T^A \times T^B = 0$.

Using the above result for $I(\vec{q})$ and writing the number of appearances of a given graph as $4^{n+1}n!/G_{n+1,g}$ we obtain the following formally exact expression for $\langle|\Delta(\vec{q})|^2\rangle$:

$$\langle|\Delta(\vec{q})|^2\rangle = \frac{1}{N_\phi}\left(\frac{k_B T}{\tilde{\alpha}}\right)^2\sum_{n=0}^{\infty}\sum_g a_{n,g}(q)(-4x)^n = \frac{1}{N_\phi}\left(\frac{k_B T}{\tilde{\alpha}}\right)^2\left\{1+N_\phi\delta_{\vec{q},0}-4x\exp\left[-\frac{q^2\ell^2}{2}\right]+4x^2\exp\left[-\frac{q^2\ell^2}{2}\right] +8x^2(1+N_\phi\delta_{\vec{q},0})+16x^2\left(0.5\exp\left[-\frac{q^2\ell^2}{4}\right]+\exp[-q^2\ell^2]\right)+\cdots\right\}, \quad (18)$$

where g labels graphs and the sum at nth order is over $(n+1)$-vertex graphs. $a_{n,g}(q)$ is given by

$$a_{n,g}(q) = \begin{cases} \frac{2}{G_{n+1,g}} \left(\frac{1}{T^A_{n,g}} \exp\left[-\frac{T^B_{n,g}}{2T^A_{n,g}} q^2 \ell^2 \right] + \frac{1}{T^B_{n,g}} \exp\left[-\frac{T^A_{n,g}}{2T^B_{n,g}} q^2 \ell^2 \right] \right) & \text{if } T^A_{n,g} \times T^B_{n,g} \neq 0, \\ \frac{2}{G_{n+1,g}(T^A_{n,g}+T^B_{n,g})} (1 + N_\phi \delta_{\vec{q},0}) & \text{if } T^A_{n,g} \times T^B_{n,g} = 0, \end{cases} \tag{19}$$

where $T^A_{n,g}$ and $T^B_{n,g}$ are the number of the Euler paths of the two contracted n-vertex graphs and $G_{n+1,g}$ is the number of automorphisms of the $(n+1)$-vertex graph with one external vertex. The diagrams which appear up to second order in the series and their associated properties are listed in Table I. The explicit expression in Eq. (18) can be confirmed from the entries in this table.

We observe in Eq. (19) that contributions which survive to the large-$|\vec{q}|$ limit come only from graphs where $T^A_{n,g}$ equals zero or $T^B_{n,g}$ equals zero and that the only terms in $\langle |\Delta(\vec{q})|^2 \rangle$ which are independent of N_ϕ come from the same set of diagrams. The contribution independent of N_ϕ is $\langle \Delta_0^2 \rangle \delta_{\vec{q},0}$. The remaining contributions to $\langle |\Delta(\vec{q})|^2 \rangle$, which are proportional to N_ϕ^{-1}, contribute to $\chi_{\rm SFD}(\vec{q})$ and are due to correlations in the thermally fluctuating superfluid density. We thus obtain explicitly from the perturbation expansion that

$$\lim_{|\vec{q}|\to\infty} \langle |\Delta(\vec{q})|^2 \rangle = \langle \Delta_0^2 \rangle / N_\phi. \tag{20}$$

This result was claimed earlier on the basis of the sum rule [Eq. (9)].

The real space correlation function is given by

$$\langle |\Psi(\vec{r})|^2 |\Psi(\vec{r}+\vec{R})|^2 \rangle = \frac{1}{(2\pi)^2} \int d\vec{q} \langle |\Delta(\vec{q})|^2 \rangle \times \exp[-q^2\ell^2/2] \exp[-i\vec{q}\cdot\vec{R}] \tag{21}$$

$$= \left(\frac{N_\phi}{L_x L_y} \right)^2 \left(\frac{k_B T}{\tilde{\alpha}} \right)^2 \times \sum_{n=0} \sum_g a_{n,g}(R)(-4x)^n; \tag{22}$$

where

$$a_{n,g}(R) = \frac{2}{G_{n+1,g} T_{n+1,g}} \left\{ \exp\left[-\frac{T^A_{n,g}}{2T_{n+1,g}} \left(\frac{R}{\ell} \right)^2 \right] + \exp\left[-\frac{T^B_{n,g}}{2T_{n+1,g}} \left(\frac{R}{\ell} \right)^2 \right] \right\}. \tag{23}$$

TABLE I. All diagrams up to second order in the high-temperature perturbation expansion. The open circle in each diagram represents the external vertex.

diagram	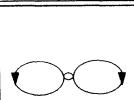	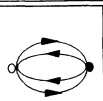			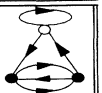
$T^A_{n,g}$	1	1	2	2	2
$T^B_{n,g}$	0	1	2	1	0
$G_{n+1,g}$	2	4	8	2	2

In Eq. (23) $T_{n+1,g} = T^A_{n,g} + T^B_{n,g}$ is the number of Euler paths in the uncontracted $(n+1)$-vertex graph. We see again here that only graphs with $T^A_{n,g} = 0$ or $T^B_{n,g} = 0$ remain finite for $R \to \infty$ where correlations vanish. The contribution of this subset of graphs is $\langle |\Psi(\vec{r})|^2 \rangle^2$.

IV. FINITE-ORDER RESULTS AND EXTRAPOLATION TO LOW TEMPERATURES

We have developed a fast graph-generation computer program which generates all relevant graphs represented by their adjacency matrices.[16] (The description of the algorithm is given in Appendix B.) From the adjacency matrices we calculate the number of Euler paths for the subgraphs ($T^A_{n,g}$ and $T^B_{n,g}$) and from the graph-generating algorithm we calculate the symmetry factor $G_{n+1,g}$. In Fig. 1, we show one of the graphs which appears at second order in the expansion, the two graphs which result from the deletion of its external vertex, and the adjacency matrices of all three graphs. (The number of Euler paths equals the determinant of the minor of the matrix appropriately formed from the corresponding adjacency matrix.[16]) In this way, we have evaluated the series exactly up to 12th order.[18] We have checked our results for $\langle |\Delta(\vec{q})|^2 \rangle$ by confirming that the sum rule Eq. (9) is satisfied and that the results for both $\langle |\Delta_0|^2 \rangle$ and $\sum_{\vec{q}} |\Delta(\vec{q})|^2 \exp\{-\frac{1}{2}q^2\ell^2\}$ are correct order by order in perturbation theory. The latter two quantities can be

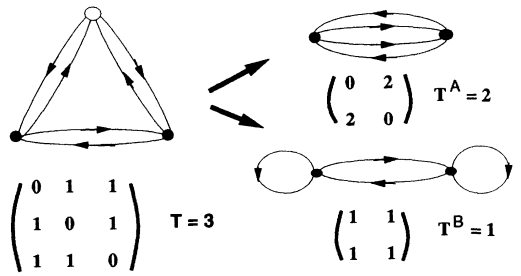

FIG. 1. Example of the adjacency matrix representation of a graph which appears at second order in the expansion and of the calculation of Euler path numbers of the graph. The graph is represented by an adjacency matrix A with elements a_{ij} where a_{ij} is equal to the number of edges going from vertex i to vertex j. The number of Euler paths is equal to the determinant of the minor of the matrix B with elements defined by $b_{ij} = \delta_{ij} \sum_k a_{ik} - a_{ij}$. The open circle in the uncontracted graphs represents the external vertex. The two graphs on the left result from the two possible contractions after deletion of the external vertex. The contribution of this graph to the series is $a_2(q) = 0.5 \exp(-q^2\ell^2/4) + \exp(-q^2\ell^2)$.

related to derivatives of the free energy. The free energy is given by

$$F = -k_B T \ln Z = k_B T N_\phi [\ln(\tilde{\alpha}/\pi k_B T) + f_{2D}(x)], \quad (24)$$

where the perturbation expansion for $f_{2D}(x)$ was first evaluated to order x^6 by Ruggeri and Thouless.[4] The expansion was extended to order x^{11} by Brézin, Fujita, and Hikami[5] and is extended to order x^{13} in the present work (see Sec. V). Differentiating Eq. (24) once with respect to β we find that

$$\sum_{\vec{q}} \langle |\Delta(\vec{q})|^2 \rangle \exp\{-\tfrac{1}{2} q^2 l^2\} = \left(\frac{k_B T}{\tilde{\alpha}}\right)^2 \times \frac{4 + (1-4x) f'_{2D}(x)}{1+4x}. \quad (25)$$

Similarly, differentiating twice with respect to α_H gives

$$\langle |\Delta_0|^2 \rangle - \langle \Delta_0 \rangle^2 = \frac{1}{N_\phi} \left(\frac{k_B T}{\tilde{\alpha}}\right)^2 \left(\frac{(1-4x)[1-2x f'_{2D}(x)]}{(1+4x)^3} - \frac{4x[f'_{2D}(x) + x f''_{2D})}{(1+4x)^2} \right), \quad (26)$$

where $\langle \Delta_0 \rangle = (k_B T/\tilde{\alpha})[1 - 2x f'_{2D}(x)]/(1+4x)$.

The following two expressions give the explicit expansions for $\langle |\Delta(\vec{G})|^2 \rangle$ and $\langle |\Delta_0|^2 \rangle$, where $|\vec{G}| = 2.693\,547 \ell^{-1}$ is the smallest reciprocal vector for the triangular lattice:

$$\begin{aligned} \langle |\Delta(\vec{G})|^2 \rangle = \frac{1}{N_\phi} \left(\frac{k_B T}{\tilde{\alpha}}\right)^2 (1 &- 0.106\,319\,841\,061\,557\,4x + 9.421\,892\,685\,500\,202\,1x^2 \\ &- 98.684\,577\,215\,755\,340\,x^3 + 1222.173\,413\,973\,232\,8x^4 - 17\,509.235\,550\,184\,578\,x^5 \\ &+ 284\,197.095\,063\,130\,49x^6 - 5\,152\,806.531\,339\,371\,6x^7 + 103\,259\,468.748\,141\,05x^8 \\ &- 2\,267\,805\,862.815\,430\,6x^9 + 54\,203\,017\,441.510\,056\,x^{10} - 1\,401\,439\,349\,032.462\,2x^{11} \\ &+ 38\,992\,399\,883\,388.438\,x^{12}) \end{aligned} \quad (27)$$

and

$$\begin{aligned} \langle |\Delta_0|^2 \rangle = \left(\frac{k_B T}{\tilde{\alpha}}\right)^2 \Bigg(1 &+ 8x^2 - \frac{248}{3}x^3 + \frac{14792}{15}x^4 - 13\,639.131\,890\,331\,891\,x^5 \\ &+ 214\,140.340\,471\,362\,08x^6 - 3\,763\,359.335\,800\,620\,3x^7 + 73\,253\,246.076\,008\,394\,x^8 \\ &- 1\,565\,815\,099.394\,278\,5x^9 + 36\,491\,644\,165.736\,839\,x^{10} - 921\,480\,933\,812.921\,26x^{11} \\ &+ 25\,075\,334\,330\,238.250\,x^{12} \Bigg). \end{aligned} \quad (28)$$

The asymptotic high-temperature expansion of $\langle |\Delta(\vec{q})|^2 \rangle$ can be extrapolated to low temperatures using Padé approximants to describe the x dependence at each value of q. Comparisons between Padé approximants of the series and our Monte Carlo simulation results[8] are given in Fig. 2 for different temperatures. $s_V(q)$ shows a well-defined peak for q near $|\vec{G}|$, where $\vec{G}$ is a reciprocal lattice vector of the vortex solid. Such a peak is characteristic of a strongly correlated liquid. Quantitative agreement with Monte Carlo simulation results is obtained for temperatures above T_c^{MF} and for temperatures below T_c^{MF} with $g^2 < 10$. A continuous phase transition to a vortex solid state at low temperatures would be indicated by the divergence of $s_V(q)$ at q near $|\vec{G}|$ and hence by a pole in the Padé approximant to $\langle |\Delta(\vec{q})|^2 \rangle$ along the positive real x axis. We find that poles do occur in some Padé approximants to $\langle |\Delta(\vec{q})|^2 \rangle$ at values of x near those at which Monte Carlo simulations find a weak first-order phase transition. However, the poles do not appear consistently in approximants of different order so the high-temperature perturbation expansion does not provide any reliable information about the temperature and the nature of the phase transition. Nevertheless we believe that the structure seen in $s_V(q)$ is a precursor of the solidification of the vortex lattice at lower temperatures. The proximity of the vortex lattice state is apparent in the perturbation theory for $s_V(q)$ but is hidden in the perturbation theory for the free energy because of the weakness of the thermodynamic singularity associated with the solidification phase transition.

V. ANALYSES OF THE FREE ENERGY EXPANSION

By developing a fast graph-generation algorithm, we were able to extend the expansion for the $f_{2D}(x)$ up to 13th order which is given by

$$\begin{aligned} f_{2D}(x) = &-2x - x^2 + \frac{38}{9}x^3 - \frac{1199}{30}x^4 + 471.396\,594\,516\,594\,46x^5 - 6471.562\,574\,955\,144\,6x^6 \\ &+ 101\,279.327\,845\,970\,63x^7 - 1\,779\,798.787\,594\,752\,2x^8 + 34\,709\,019.614\,363\,678\,x^9 \\ &- 744\,093\,435.668\,222\,31x^{10} + 17\,399\,454\,123.559\,521\,x^{11} \\ &- 440\,863\,989\,257.285\,10x^{12} + 12\,035\,432\,945\,204.531\,x^{13}. \end{aligned} \quad (29)$$

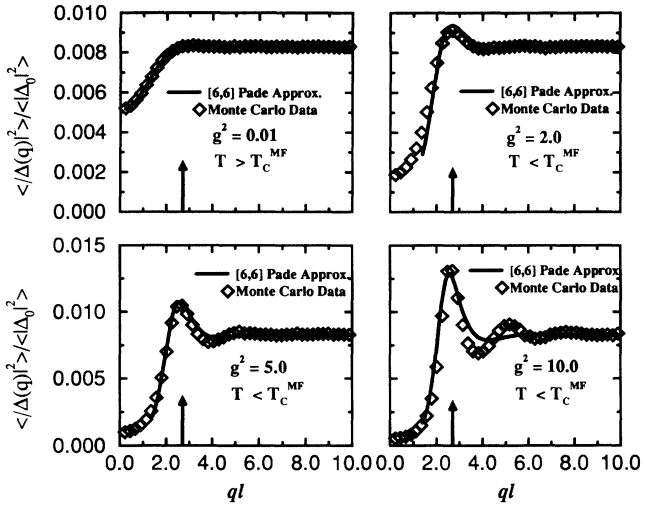

FIG. 2. Comparisons of the perturbation calculation and Monte Carlo simulations. The y-axis label is $\langle|\tilde{\Delta}(\vec{q})|^2\rangle$, while the x axis is wave vector in the units of the inverse magnetic length ℓ^{-1}. The upper-left panel is for a temperature above $T_c^{\rm MF}$, while the other panels are for temperatures below $T_c^{\rm MF}$. The arrows in the plots indicate the location of reciprocal vector $|\vec{G}|$ of the vortex lattice state. The Padé approximants sometimes behave poorly at small wave vectors due to the existence of the defect poles around $q\ell \sim 1.0$. We have "clipped" anomalous small-wave-vector behavior in some of these figures so as not to obscure the behavior for q near G.

The Abrikosov ratio β_A, which measures the average smoothness of the superfluid density, can be obtained in term of $f_{2D}(x)$ as

$$\beta_A = \frac{[4+(1-4x)f'_{2D}(x)](1+4x)}{[1-2xf'_{2D}(x)]^2}. \tag{30}$$

In the low-temperature (large-x) limit, the $f_{2D}(x)$ is linear in x, $f_{2D}(x) = -ax$, and the Abrikosov ratio β_A is given by $4/a$. The high-temperature expansion results for $f_{2D}(x)$ can be extrapolated to the large-x limit by using the $[n, n-1]$ Padé approximants for the expansion series. The resulting low-temperature limits for the Abrikosov ratio β_A obtained by [4,3], [5,4], [6,5], and [7,6] Padé approximants are 1.398 94, 1.298 72, 1.256 67, and 1.240 57, respectively. The [7,6] approximant requires the high-temperature expansion to be known to order x^{13} and so was not previously available. Figure 3 shows the low-temperature limits of the approximants. The dashed line shows an extrapolation of the low-temperature limits of the $[n, n-1]$ approximants for $n = 4$, $n = 5$, and $n = 6$ to $n = \infty$, which suggests that the high-temperature expansion if carried out to sufficiently high order could provide an accurate estimate of the zero-temperature β_A and hence the zero-temperature free energy as has been

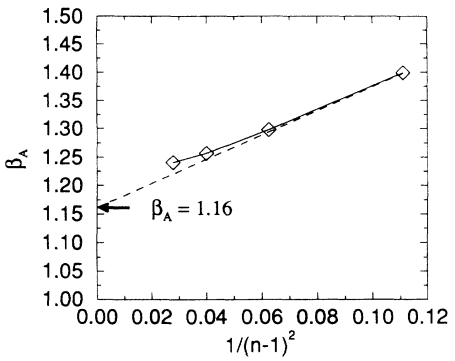

FIG. 3. The extrapolation of the Abrikosov ratio β_A by $[n, n-1]$ Padé approximants ($n = 4$, 5, 6, and 7).

argued by Hikami, Fujita, and Larkin.[5] (At zero temperature $\beta_A \sim 1.16$.) However the newly available $n = 7$ $[n, n-1]$ approximant clearly deviates from this extrapolation.

VI. SUMMARY AND CONCLUSIONS

We have studied the superfluid-density spatial correlation function $\langle|\Delta(\vec{q})|^2\rangle$ using high-temperature perturbation expansions and extrapolated our results to temperatures below the mean-field transition temperature by means of Padé approximants. Good agreement with Monte Carlo simulation data is obtained for $g > -\sqrt{10}$. Our results demonstrate that the vortex liquid is strongly correlated below $T_c^{\rm MF}$. A result argued for previously on the basis of a sum rule which related the large-wave-vector limit of the correlation function to the average superfluid density was obtained explicitly from the perturbation expansion. We argue that these perturbation expansion studies give clear indications of the phase transition to a two-dimensional vortex solid that is believed to occur at lower temperatures, although they cannot at present provide reliable information about the nature of the phase transition or the temperature at which it occurs. We have also evaluated two more orders in the high-temperature expansion of the free energy. These results demonstrate that caution needs to be exercised when extrapolating low-temperature results because of the slow convergence of the series.

ACKNOWLEDGMENTS

This work was supported by the Midwest Superconductivity Consortium through DOE Grant No. DE-FG-02-90ER45427. The authors are grateful to Steve Girvin and Lian Zheng for helpful interactions.

APPENDIX A

The integral to be evaluated has the form

$$I(\vec{q}) \equiv e^{-il^2 q_y(q_x+iq_y)}\left(\frac{2\pi}{\ell^2}\right)^{-n/2}\sum_{p_2}\int dp_3\cdots\int dp_{2n+2}\prod_{\mu=2}^{n+1}\delta\left(\sum_i (M_{\mu i}-N_{\mu i})p_i\right)$$
$$\times(\delta_{p'_1+q_y}+\delta_{p'_2+q_y})e^{-i\ell^2(q_x+iq_y)p_2}\exp\left\{-\frac{\ell^2}{2}\sum_{\mu=2}^{n+1}(p_{2\mu}-p_{2\mu-1})^2\right\}. \tag{A1}$$

Of the $(2n+1)$ variables p_i only n are independent because of the $(n+1)$ δ functions. It is convenient[15] to choose $s_\mu = p_{2\mu} - p_{2\mu-1}$ $(\mu = 2,\ldots,n+1)$ as the n independent variables. We label the contributions to $I(\vec{q})$ from the two choices for the δ function at the external vertex as $I^A(\vec{q})$ and $I^B(\vec{q})$ respectively. We use this δ function to eliminate the sum over $p_2 = s_1$ which can then be expressed as a linear function of the independent variables. For $X = A$ or B

$$s_1^X = -\alpha^X q_y + \sum_{\mu=2}^{n+1} t_\mu^X s_\mu. \tag{A2}$$

The integral over the independent variables can then be expressed in terms of these coefficients. The Jacobian for changing variables from p_μ to $s_{\mu>1}$ is independent of q_y; at $q_y = 0$ the change of variables is identical to that required for the diagram obtained by deleting the external vertex and contracting the two outgoing edges at that vertex with the two incoming edges. [The two ways of doing the contraction correspond to $I^A(\vec{q})$ and $I^B(\vec{q})$ respectively.] Following the work of McCauley and Thouless[15] we note that the inverses of the required Jacobians equal the number of Euler paths[16] for the n-vertex graphs which results from the deletion of the external vertex and the two possible contractions. We denote the Euler path numbers by T^X. The integral over the s_μ is then elementary and we obtain

$$I^X(\vec{q}) = (e^{i\ell^2 q_x q_y})^{n_1^X} (e^{-\ell^2|q_y|^2})^{n_2^X} (e^{-\ell^2|q_x|^2})^{n_3^X} \frac{1}{T^X}, \tag{A3}$$

where $n_1^X = -1 + \alpha^X - \sum_{\mu=2}^{n+1}(t_\mu^X)^2$, $n_2^X = -1 + \alpha^X - \frac{1}{2}\sum_{\mu=2}^{n+1}(t_\mu^X)^2$, and $n_3^X = \frac{1}{2}\sum_{\mu=2}^{n+1}(t_\mu^X)^2$. However, we know that $I^X(\vec{q})$ is real, which leads to the requirement that $n_1^X = 0$ and implies that $I^X(\vec{q}) = \exp[-q^2\ell^2(\alpha^X - 1)/2]/T^X$. The value of α^X can be inferred by noting that $\sum_q \exp(-q^2\ell^2/2) I^X(\vec{q})$ is proportional to an integral which appears in the expansion of the free energy and equals N_ϕ/T where T is the number of Euler paths in the original graph before deletion. It follows that $\alpha^X = T/T^X$ and hence that

$$I(\vec{q}) = \left\{ \frac{1}{T^A} \exp\left(-\frac{T^B}{2T^A} q^2\ell^2\right) + \frac{1}{T^B} \exp\left(-\frac{T^A}{2T^B} q^2\ell^2\right) \right\}. \tag{A4}$$

(Note that $T^A + T^B = T$.) This analysis fails in the special case where $T^A \times T^B = 0$. For that case we have $I^X(\vec{q}) = n^X \delta_{\vec{q},0}$ or $I^X(\vec{q}) = n^X$ and a similar analysis gives the corresponding $n^X = N_\phi/T$ or $n^X = 1/T$, and so

$$I(\vec{q}) = (N_\phi \delta_{\vec{q},0} + 1)/(T^A + T^B). \tag{A5}$$

APPENDIX B

In this appendix we give a description of the algorithm used to generate the required diagrams. Define a *basic digraph* to be a directed graph with each vertex having two incoming edges and two outgoing edges. Loops are forbidden, but parallel edges (edges with the same head and tail) are permitted. Connectivity is not required at this stage, nor is there a vertex distinguished from the others.

Our first task is to generate representatives of the isomorphism classes of basic digraphs with at most 13 vertices. Since there are more than 200 million such classes, we need a method which does not require storage of all the graphs at once. The necessary tools are provided by a computer program developed by one of us.[17] For an arbitrary digraph, this program can assign a canonical labeling to the vertices and find a set of generators for the automorphism group.

Let g be a basic digraph. Let v be a vertex of g, with incoming edges (u_1, v) and (u_2, v) and outgoing edges (v, w_1) and (v, w_2). We can form a smaller digraph by deleting v and replacing the four incident edges by either (u_1, w_1) and (u_2, w_2), or (u_1, w_2) and (u_2, w_1). These *unwelding* operations will be called *legal* if they do not create loops. The inverse of an unwelding is, of course, a *welding*. It consists of taking two edges and welding their midpoints together to form a new vertex.

The idea is to generate the basic digraphs by performing welding operations on smaller basic digraphs, beginning with those which admit no legal unweldings. The latter class, called *primitive*, are easily identified as those whose connected components all lie in the class $\{P_1, P_2, \ldots\}$. Here, P_m is the basic digraph with vertices $v_0, \ldots, v_{2m-1}$ and edges (v_i, v_{i+1}) for $i = 0, \ldots, 2m-1$ and two each of the edges (v_{2i}, v_{2i-1}) for $i = 1, \ldots, m$, where $v_{2m} = v_0$.

Let g be a basic digraph which is not primitive. In order to avoid generation of many isomorphs of g, we define a set $U(g)$ of *major* unwelding operations. The required properties are that $U(g)$ is an equivalence class of legal unweldings under the automorphism group of g, and that $U(g)$ is independent of the labeling of g in the sense that $U(g^\gamma) = U(g)^\gamma$ for every relabeling γ. For reasons of efficiency, we defined $U(g)$ by first choosing those legal unweldings which maximized a combinatorial invariant based on distances, then, in the exceptional cases where this failed to identify a single unwelding, used NAUTY to choose canonically a first legal unwelding and defined $U(g)$ to be its equivalence class. The defining properties ensure that, if g_1 and g_2 are isomorphic basic digraphs with major unweldings $\phi_1 \in U(G_1)$ and $\phi_2 \in U(g_2)$, then $\phi_1(g_1)$ and $\phi_2(g_2)$ are isomorphic.

We can now describe the generation process. Suppose we have representatives of the isomorphism classes of basic digraphs of order n. For each such digraph g, we perform exactly those weldings whose inverses are major unweldings. This restriction ensures that isomorphic basic digraphs can only appear within the set of offspring of the same g, so we can eliminate them by comparing the new digraphs only to their siblings. (In fact, such iso-

TABLE II. Number of connected basic digraphs for each order up to 13.

3	4	5	6	7	8	9	10	11	12	13
2	5	13	59	285	1987	16057	149430	1551863	17747299	221015026

morphs only arise from the symmetries of g, but we chose not to use that fact.) After this local isomorph rejection is complete, we have exactly one representative from each equivalence class of basic digraphs of order $n+1$, except for the primitive digraphs. The latter are easily added separately. The number of connected basic digraphs of each order up to 13 are shown in Table II.

The diagrams required for the expansion are easily made from the basic digraphs. Recall that the diagrams are connected, have a distinguished "external" vertex labeled separately (and allowed to carry a loop), and have an ordering specified for the two incoming edges at each vertex and for the two outgoing edges. Suppose g is a connected basic digraph with automorphism group having order G (including interchange of parallel edges) and vertex orbits $O_1, \ldots, O_t$. We can make diagrams with $n+1$ vertices in two distinct ways.

To make diagrams with no loops, choose any g with $n+1$ vertices. Then choose any orbit O_i and designate an arbitrary vertex of that orbit to be the external vertex. The number of labeled diagrams in this class is $n!\,|O_i|4^{n+1}/G$.

To make diagrams with the external vertex carrying a loop, choose g to have $n-j+1$ vertices for some $j \geq 1$ and delete some edge $e = (v, w)$. Append new vertices $u_1, \ldots, u_j$ and new edges (v, u_1), (u_1, w), (u_i, u_{i+1}), (u_{i+1}, u_i) $(1 \leq i \leq j-1)$, and (u_j, u_j). Vertex u_j becomes the external vertex. The number of corresponding labelled diagrams depends on the action of the automorphism group of g on the edge e. However, since the number of Euler paths in the resulting diagram does not depend on e, we can group together all the diagrams derivable from g in this manner. The total number of labeled diagrams in this class is $2(n+1)!\,4^{n+1}/G$.

[1] A. A. Abrikosov, Zh. Eksp. Teor. Fiz. **32**, 1442 (1957) [Sov. Phys. JETP **5**, 1174 (1957)].

[2] D. R. Nelson, Phys. Rev. Lett. **60**, 1415 (1988); P. L. Gammel, L. F. Schneemeyer, J. V. Wasczak, and D. J. Bishop, *ibid.* **61**, 1666 (1988).

[3] P. A. Lee and S. R. Shenoy, Phys. Rev. Lett. **28**, 1025 (1972).

[4] G. J. Ruggeri and D. J. Thouless, J. Phys. F **6**, 2063 (1976).

[5] E. Brézin, A. Fujita, and S. Hikami, Phys. Rev. Lett. **65**, 1949 (1990); S. Hikami, A. Fujita, and A. I. Larkin, Phys. Rev. B **44**, 10 400 (1991).

[6] Zlatko Tešanović and L. Xing, Phys. Rev. Lett. **67**, 2729 (1991).

[7] Yusuke Kato and Naoto Nagaosa, Phys. Rev. B. **47**, 2932 (1993).

[8] Jun Hu and A. H. MacDonald, Phys. Rev. Lett. **71**, 432 (1993).

[9] J. A. O' Neill and M. A. Moore, Phys. Rev. B **48**, 374 (1993).

[10] A. H. MacDonald, Hiroshi Akera, and M. R. Norman, Aust. J. Phys. **46**, 333 (1993).

[11] The limits of validity of this approximation are discussed by Ryuske Ikeda (unpublished).

[12] We also neglect fluctuations in the vector potential. This approximation is permitted as long as the temperature is not too far below the mean-field transition temperature or the films are thin and widely separated.

[13] We remark that Eq. (9) is exact even for finite-size systems with quasiperiodic boundary conditions applied to the order parameter. In that case the number of $\vec{q}$ values in the sum over wave vectors is N_ϕ^2. Finite-size effects have to be considered carefully when terms of order N_ϕ^{-1} are retained on the left hand side of Eq. (9).

[14] Giorgio Parisi, *Statistical Field Theory* (Addison-Wesley, New York, 1988).

[15] G. P. McCauley and D. J. Thouless, J. Phys. F **6**, 109 (1976).

[16] C. W. Marshall, *Applied Graph Theory* (Wiley-Interscience, New York, 1971).

[17] B. D. McKay, Australian National University, Technical Report No. TR-CS-90-02, 1990 (unpublished).

[18] The perturbation expansion of the Fourier transform of this function has previously been evaluated to sixth order using a different approach by Ryuske Ikeda, Tetsuo Ohmi, and Toshihiko Tsuneto [J. Phys. Soc. Jpn. **59**, 1397 (1990)].